THE ASTROPHYSICAL JOURNAL, 345:543–553, 1989 October 1


# CHROMOSPHERIC STRUCTURE OF COOL CARBON STARS

DONALD G. LUTTERMOSER[1] AND HOLLIS R. JOHNSON
Indiana University
AND
EUGENE H. AVRETT AND RUDOLF LOESER
Center for Astrophysics
*Received 1988 August 31; accepted 1989 March 8*

## ABSTRACT

We generate a semiempirical chromospheric model for TX Psc representing a prototype for the N-type carbon stars. We solve self-consistently in a plane-parallel geometry the statistical equilibrium and radiative transfer equations for H, $H^-$, $H_2$, C I, C II, Na I, Mg I, Mg II, Ca I, and Ca II and generate synthetic spectra. The synthetic fluxes of the Mg II *h* and *k* lines are calculated in complete and partial redistribution and compared with a high-resolution *IUE* spectrum. Synthetic fluxes from the C II] (UV 0.01) multiplet are also generated and compared with low-resolution *IUE* spectra. Calculations are made in hydrostatic equilibrium, but the effects on the Mg II lines from an assumed chromospheric velocity field are also investigated. To match the observations, we find that (1) the chromospheric temperature rise must begin at a low density ($\sim 10^{-11}$ g $cm^{-3}$); (2) the temperature gradient in the lower chromosphere must be steep, (3) Ca I ($4p\,^3P^o$) bound-free opacity must be included to reproduce the continuum levels in the vicinity of Mg II; (4) partial redistribution must be used in the Mg II calculations; (5) the lower chromosphere is expanding away from the photosphere with velocities near 50 km $s^{-1}$, but the upper chromosphere is nearly static with respect to the photosphere; (6) the microturbulent velocity is near 7 km $s^{-1}$ at the temperature minimum region but drops to 5 km $s^{-1}$ in the chromosphere; and (7), although the Lyman lines are optically thick in the chromosphere, these lines are not in detailed balance and this effect is important to the electron density.

*Subject headings:* radiative transfer — stars: carbon — stars: chromospheres — stars: individual (TX Psc)

## I. INTRODUCTION

Considerable information is available regarding chromospheres and coronae of intermediate (G–K) stars, but red giants of types M, S, and C have only recently begun to receive attention (e.g., Hartmann and Avrett 1984; Johnson 1987; Luttermoser *et al.* 1987; Eaton and Johnson 1988; Judge 1989). We report here an investigation of the chromospheric structure of some of the coolest stars in the sky—the non-Mira N-type carbon stars. These stars were shown to have chromospheres by the discovery of emission features of Fe II in the violet spectral region (Bidelman and Pyper 1963) and of C II, Mg II, and Fe II in the long-wavelength region of the *International Ultraviolet Explorer* (*IUE*) (Johnson and O'Brien 1983; Querci and Querci 1983). The obvious weakness of the ultraviolet emission-line fluxes of the carbon stars compared with M giant stars has been documented in the form of color-color diagrams of Mg II *h* and *k* emission as a function of $V-K$ for a variety of late stars (Eaton *et al.* 1985; Johnson 1987); fractional Mg II emission strength decreases steadily with advancing spectral types for the oxygen-rich stars, and the emission for the N-type carbon stars is comparable to that of the M7–M8 giants.

All low-resolution, long-wavelength *IUE* spectra for seven N-type carbon stars have been systematically studied for line identifications (Johnson and Luttermoser 1987). The blended Mg II *h* and *k* lines are the strongest emission features, followed by C II] (UV 0.01); a plethora of Fe II emission lines cover the spectra as well.

A high-resolution *IUE* spectrum has been obtained for only one N-type carbon star—TX Piscium (Eriksson *et al.* 1986). The 13.5 hr observation showed a substantial amount of circumstellar absorption overlying the Mg II *h* and *k* lines and suggests that part of the relative weakness of the Mg II fluxes may be that carbon stars have more overlying absorbing material than do M stars. This high-resolution spectrum was bracketed by two low-resolution *IUE* spectra (Johnson *et al.* 1986) as described in § II.

As a prelude to *chromospheric* modeling, Johnson, Luttermoser, and Faulkner (1988) generated synthetic spectra for cool supergiant star *photospheres* with emphasis on TX Psc. These authors proposed, and computed synthetic spectra to demonstrate, a new solution to the "violet opacity problem" in carbon stars; the steep falloff in violet flux is due to the cumulative effect of several opacity sources, primarily bound-bound and bound-free opacities from the ground and metastable states of neutral metals, particularly Mg I, Ca I, and Fe I absorption lines and Na I, Mg I, and Ca I photoionizations, and to a lesser extent, CH photodissociation and the $C_3$ pseudocontinuum. They found the violet flux falloff to be primarily an effect of temperature and not composition, although carbon abundance plays an indirect role in determining the amount and depth of CO cooling.

Exploratory chromospheric modeling of TX Psc was attempted by Avrett and Johnson (1984), who were able to produce Mg II emission lines, but at smaller fluxes than observed. The present paper greatly extends that initial work.

We try to determine the chromospheric temperature-density structure of TX Psc with a semiempirical approach. We start by attaching an estimated temperature rise to the outer layers of a radiative equilibrium model photosphere to simulate a chromosphere. A synthetic spectrum is generated for the model

[1] Now at the Joint Institute for Laboratory Astrophysics, University of Colorado.

and is compared with available observations. The temperature-density stratification then is altered until the observations can be reproduced.

Section III presents non–LTE calculations with the PANDORA stellar atmosphere code (Vernazza, Avrett, and Loeser 1973, 1976, 1981) including both complete redistribution (CRD) and partial redistribution (PRD). Comparisons are made with the high-resolution spectrum of Mg II *h* and *k* lines and the C II] (UV 0.01) integrated line fluxes from the low-resolution *IUE* spectra of TX Psc. Section IV describes synthetic flux calculations of Mg I (2852 Å), Ca II H and K, and Hα for the chromospheric model derived from the Mg II *h* and *k* lines. Section V summarizes our results.

## II. OBSERVATIONS

Because of the observational data available, TX Psc is an ideal prototype for the investigation of N-type carbon star chromospheres. Photometric and spectral observations of this star in the visual and infrared have been reviewed by Faulkner, Honeycutt, and Johnson (1988) and Johnson, Luttermoser, and Faulkner (1988). The dominant spectral features in the visual and near-infrared are the CN red system bands and the Na D doublet. The $C_2$ bands shortward of 5700 Å are relatively weaker than in other N-type stars. Consistent with other N-type irregular (Lb) variables, Balmer lines are not seen either in absorption or in emission (Yamashita 1972, 1975), although Hα lies among many strong CN lines and a weak feature might be present. The lack of strong Balmer features is puzzling, since TX Psc, along with the six other N-type irregular variable stars observed with *IUE*, display emission lines from singly ionized metals in their low-resolution ultraviolet spectra (Johnson and Luttermoser 1987). Such emission lines are generally considered chromospheric indicators, and such a temperature rise in the outer layers of this star might be expected to produce Balmer lines.

The traditional chromospheric indicators for main-sequence stars and oxygen-rich giants and supergiants are the Ca II H and K lines. These resonance lines display emission peaks in the line core due to the chromospheric temperature increase and the coupling between the line source function and the Planck function. Richer (1975) recorded H and K in absorption in several carbon stars but could not resolve the bottoms of the lines. However, P. Bouchet (1982, private communication) was able to detect the deepest portions of the H and K lines on an overexposed spectrum of TX Psc but found no reversal in the line profiles.

The radial velocity has been determined by Abt and Biggs (1972) to be $+12 \pm 4$ km s$^{-1}$ from photospheric lines. Eriksson *et al.* (1986) tabulate velocity measurements from the emission lines seen in the high-resolution *IUE* spectrum and from the CO $J = 1$–0 (115.271 GHz) line.

Table 1 lists a summary of the three *IUE* spectra used in our non–LTE study. The low-resolution spectra show emission lines shortward of 2850 Å with the two strongest features being Mg II (UV 1) near 2800 Å and C II] (UV 0.01) near 2325 Å, respectively. Identifications of the other emission features have already been published (Johnson and Luttermoser 1987).

The C II] lines near 2325 Å are the transitions between the $2s^2 2p\ ^2P^o$ and $2s2p^2\ ^4P$ states. These optically thin lines have been shown to be electron density diagnostics in stellar atmospheres (e.g., Stencel *et al.* 1981; Lennon *et al.* 1985). Although they are the second strongest emission features in the low-resolution *IUE* spectra, they are too faint to appear on the high-resolution *IUE* spectrum, and consequently we cannot deduce the electron density. However, we can use the integrated flux of these lines from the low-resolution spectra as a check of the temperature-density stratification determined from the Mg II lines. Table 1 also lists the integrated flux of C II] (UV 0.01) and Mg II (UV 1) as measured from the *IUE* spectra.

TABLE 1

SUMMARY OF *IUE* OBSERVATIONS OF TX PISCIUM (1984 May 31)

| *IUE* Exposure | Exposure Time (minutes) | Spectral Resolution[a] Å | Flux[b] C II][c] | Flux[b] Mg II[d] |
|---|---|---|---|---|
| LWP 3468..... | 60 | 6 | 26[e] | 59[f] |
| LWP 3469..... | 810 | 0.3 | not seen | 67 |
| LWP 3470..... | 60 | 6 | 32[e] | 60 |

[a] Grady 1987.
[b] Flux observed from Earth ($10^{-14}$ ergs s$^{-1}$ cm$^{-2}$).
[c] C II] (UV 0.01) near 2325 Å.
[d] Mg II (UV 1, *h* and *k*) near 2800 Å.
[e] Noisy spectral region.
[f] Slightly saturated (10% loss?).

The Mg II *h* and *k* lines (i.e., multiplet UV 1) are the resonance transitions of this ion ($3s^2\ ^2S$–$3s3p\ ^2P^o$) at $\lambda_{air} = 2795.523$ Å and 2802.698 Å and are the normal chromospheric indicators. Since Mg is approximately 17 times as abundant as Ca in a solar mixture, and both Mg I and Ca I are easy to ionize (7.1 and 6.1 eV, respectively), *h* and *k* are expected to show the effects of a chromospheric temperature rise to a greater degree than H and K. The Mg II emission profiles in the high-resolution *IUE* spectrum are blueshifted with respect to the central self-absorption and are strongly affected by circumstellar absorption—especially on the short-wavelength side of the *k* line. Most of the circumstellar absorption is due to the resonance transitions of Mn I (UV 1), Fe I (UV 3), and Mg II self-absorption (Eriksson *et al.* 1986). The only portion of the Mg II emission unaffected by circumstellar absorption is the short-wavelength side of the *h* line.

It is virtually impossible to determine the amount of interstellar absorption in the Mg II *h* and *k* lines of TX Psc because of the large amount of circumstellar absorption from Mn I and Fe I overlying these lines and because of the noise of the spectrum. TX Psc has no noticeable interstellar reddening: Walker (1980) has determined $E(B-V)$ to be zero. Bohlin, Savage, and Drake (1978) have found the ratio of hydrogen column mass to reddening in the interstellar medium (ISM) to be roughly constant. Accordingly, the amount of interstellar absorption over these lines may be small. We will discuss the possible effects of interstellar absorption on the Mg II line profiles in § III*c*.

TX Psc has a measured angular diameter (mean of three observations) of $9.31 \pm 0.75$ mas by lunar occultation (cf. Ridgway, Wells, and Joyce 1977; White and Feierman 1987). This allows *absolute* flux comparisons to be made between the synthetic and the observed fluxes. Ridgway, Wells, and Joyce (1977) also determined the effective temperature from the measured angular diameter and bolometric flux to be $3080 \pm 150$ K. Tsuji (1981) and Lambert *et al.* (1986) review effective temperatures for TX Psc and other N-type carbon stars derived by a variety of different authors.

The chemical composition of TX Psc has been determined by Lambert *et al.* (1986). For the adopted values of $T_{eff} = 3030$ K and the photospheric microturbulent velocity of 2.2 km s$^{-1}$,

they find $^{12}C/^{13}C = 43$, $(^{12}C + ^{13}C)/O = 1.027$, $[(^{12}C + ^{13}C)/H] = +0.16$, $[^{14}N/H] = -0.27$, $[^{16}O/H] = -0.10$, [Ca/H] $= -0.3$, and [Fe/H] $= -0.4$, where $[X/H] = \log (X/H) - \log (X/H)_\odot$. Except for carbon, all elements are slightly underabundant with respect to the Sun, but the abundances are similar to those of K and M giants except for nitrogen, which is underabundant in carbon stars with respect to K and M giants (Smith and Lambert 1985; Lambert *et al.* 1986).

The surface gravity of TX Psc is the most uncertain input parameter. The measured angular diameter can be used to determine a linear diameter from its distance. N-type carbon stars in the Large Magellanic Cloud appear to have approximately the same absolute $K$-magnitude of $-8.2$ (Cohen *et al.* 1981). Using the apparent $K$-magnitude of TX Psc ($-0.76$) and the assumption that N stars in the Milky Way and the LMC have similar brightness, the distance to TX Psc is approximately 300 pc and the linear radius is 300 $R_\odot$. The masses of N-type carbon stars have been estimated by Aaronson and Mould (1985) and Catchpole and Feast (1985) to be approximately 2 $M_\odot$. This corresponds to $\log g \simeq -0.2$. For convenience, and compatibility with the existing grid of radiative equilibrium models, we adopt $\log g = 0$.

### III. RADIATIVE TRANSFER CALCULATIONS

The chromospheric temperature-density structure is determined with a semiempirical technique. We first attach a chromospheric temperature model onto the outer layers of a representative model photosphere and calculate a corresponding density model from hydrostatic equilibrium, including a proper treatment of ionization and recombinations. A synthetic spectrum is then computed. The chromospheric temperature-density stratification is altered until the synthetic flux matches the *IUE* flux. For TX Psc we use a plane-parallel radiative equilibrium atmosphere from the "Indiana" grid of photospheric models with $T_{\rm eff} = 3000$ K, $g = 1$ cm s$^{-2}$, and solar abundances except that the carbon abundance is enhanced to achieve a carbon-to-oxygen ratio of 1.05 (Johnson 1982). Synthetic flux from the photospheric model has already been shown to reproduce the visual and infrared flux of TX Psc fairly well (Johnson, Luttermoser, and Faulkner 1988), and simple LTE flux calculations of a preliminary chromospheric model of this star approximately reproduce the long-wavelength prime (LWP) low-resolution spectra of this star (Luttermoser *et al.* 1987). We use this preliminary "LTE" chromospheric model as our initial model for the non–LTE calculations.

We solve the radiative transfer and statistical equilibrium equations with the PANDORA program (Vernazza, Avrett, and Loeser 1973, 1976, 1981) in a horizontally homogeneous, plane-parallel atmosphere. Because the equations and techniques used in PANDORA are described in detail in the three papers by Vernazza, Avrett, and Loeser listed above, we describe only recent relevant additions to the code.

We use the following initial iterative procedure for the flux calculations: (1) The combined statistical equilibrium and radiative transfer equations were first solved for a 3 level H atom with Ly$\alpha$ and Ly$\beta$ assumed to be in detailed balance and with $J_\nu = W(z)B_\nu[T_{\rm rad}(z)]$ for the hydrogen Balmer and Paschen continua, where $W(z)$ is the geometric dilution factor. We take $W = 0.5$ and $T_{\rm rad} = 3000$ K for $z \leq -4.7 \times 10^6$ km (i.e., the chromosphere), $W = 1$ and $T_{\rm rad} = T_e$ for $z \geq -8 \times 10^4$ km (i.e., near $\tau_{5000\,\text{Å}} = 1$), and $W$ is linearly interpolated with respect to the depth between the values of $z$ listed above. Hydrostatic equilibrium then gives the total density as a function of height ($z = 0$ is set at unit continuum optical depth at 5000 Å). We iteratively determine a consistent set of level populations, source functions, and net radiative rates in these calculations. (2) We then solve the coupled statistical equilibrium and radiative transfer equations for the following multilevel atoms and ions: C I (10 levels), C II (7 levels), Ca I (8 levels), Ca II (6 levels), Na I (8 levels), Mg I (7 levels), and Mg II (6 levels). All other species are assumed in LTE. (3) Finally we solve the equations for a 4 level H atom with all the lines treated in detail, and $J_\nu$ for the continuum determined by solving the transfer equation. The entire system is re-solved iteratively to obtain a consistent solution for a given temperature distribution. The calculations are then repeated with different temperature distributions until the observed spectral features are reproduced.

The atoms and ions specified above were chosen for our non–LTE analysis for the following reasons: (1) C I is the dominant electron contributor in the middle chromosphere; (2) C II provides the multiplet at 2325 Å; (3) Ca I has strong bound-free opacities in the *IUE* wavelength regime; (4) Ca II resonance lines are chromospheric indicators (although emission has not been observed in these lines for this star); (5) Na I is the dominant electron contributor throughout most of the photosphere and has a strong bound-free opacity edge at 2413 Å; (6) Mg I is the dominant electron contributor in the temperature minimum region, it has a strong bound-free opacity edge at 2514 Å, and its resonance line at 2852 Å is an important opacity source in the *IUE* long-wavelength range (Johnson, Luttermoser, and Faulkner 1988); and (7) the resonance lines of Mg II are the primary chromospheric indicator for this study.

H I.—The 4 level atom includes the four lowest energy levels of the hydrogen atom in the statistical equilibrium equations; the six bound-bound radiative transitions between these states are also included. The 3 level model includes the three lowest energy levels. Initially we solve the line transfer equation only for H$\alpha$, and assume detailed balance for Ly$\alpha$ and Ly$\beta$. This assumption is later relaxed in the 3 level case before we use the 4 level atom.

C I.—This 10 level model includes the following levels: (1) $2s^2 2p^2\,^3P$, (2) $2p^2\,^1D$, (3) $2p^2\,^1S$, (4) $2p^3\,^5S^o$, (5) $3s^3P^o$, (6) $3s^1\,^1P^o$, (7) $2p^3\,^3D^o$, (8) $3pS$, $P$, $D$, (9) $2p^3\,^3P^o$, and (10) $2p^3\,^3S^o$. Nine bound-bound radiative transitions include (upper level–lower level) 4–1, 5–1, 5–2, 5–3, 6–2, 6–3, 7–1, 8–5, and 9–1, (cf. Fig. 2 of Vernazza, Avrett, and Loeser 1981).

C II.—This 7 level model includes (1) $2s^2 2p\,^2P_{1/2}$, (2) $2p\,^2P_{3/2}$, (3) $2p\,^4P_{1/2}$, (4) $2p\,^4P_{3/2}$, (5) $2p\,^4P_{5/2}$, (6) $2p^2\,^2D_{3/2}$, and (7) $2p^2\,^2D_{5/2}$, and eight bound-bound radiative transitions: 3–1, 3–2, 4–1, 4–2, 5–2 (these are the UV 0.01 multiplet), 6–2, 7–1, and 7–2.

Na I.—This 8 level model includes (1) $3s^2S$, (2) $3p\,^2P^o_{1/2}$, (3) $3p\,^2P^o_{3/2}$, (4) $4s\,^2S$, (5) $3d\,^2D_{5/2}$, (6) $3d\,^2D_{3/2}$, (7) $4p\,^2P^o_{1/2}$, and (8) $4p\,^2P^o_{3/2}$, and eleven bound-bound radiative transitions: 2–1, 3–1 (D lines), 4–2, 4–3, 5–3, 6–2, 6–3, 7–1, 7–4, 8–1, and 8–4.

Mg I.—This 7 level model includes (1) $3s^2\,^1S$, (2) $3p\,^3P^o$, (3) $3p\,^1P^o$, (4) $4s\,^3S$, (5) $4p\,^3P^o$, (6) $3d\,^3D$, and (7) $4d\,^3D$, and seven transitions: 2–1, 3–1, 4–2, 5–4, 6–2, 7–2, and 7–5.

Mg II.—This 6 level model includes (1) $3s\,^2S$, (2) $3p\,^2P^o_{1/2}$, (3) $3p\,^2P^o_{3/2}$, (4) $4s\,^2S$, (5) $3d\,^2D$, and (6) $5s\,^2S$, and the transitions 2–1, 3–1, ($h$ and $k$, respectively), 4–2, 4–3, 5–3, 6–2, and 6–3.

Ca I.—This 8 level model includes (1) $4s^2\,^1S$, (2) $4p\,^3P^o_{3/2}$, (3) $4p\,^3P^o_{5/2}$, (4) $3d\,^3D$, (5) $3d\,^1D$, (6) $4p\,^1P^o$, (7) $5s\,^3S$, and (8) $4p'\,^1P^o$.

Six radiative transitions include 2–1, 6–1, 7–2, 7–3, 8–1, and 8–5.

Ca II.—This 5 level model includes (1) $4s\ ^2S$, (2) $3d\ ^2D_{3/2}$, (3) $3d\ ^2D_{5/2}$, (4) $4p\ ^2P^o_{1/2}$, and (5) $4p\ ^2P^o_{3/2}$, and the five transitions 4–1, 5–1 (H and K, respectively), 4–2, 5–2, and 5–3 (the infrared triplet).

*a) Complete Redistribution in a Static Atmosphere*

In the first stage of the non–LTE calculations we make the assumptions of CRD in a static atmosphere for all radiative transitions. The monochromatic source function is defined by

$$S_\nu = \frac{\phi_\nu}{\phi_\nu + r_\nu} S^l_\nu + \frac{r_\nu}{\phi_\nu + r_\nu} S^c_\nu , \quad (1)$$

where $\phi_\nu$ is the line profile normalized such that

$$\int_0^\infty \phi_\nu \, d\nu = 1 , \quad r_\nu = \phi_{\nu_0}(\chi^c_\nu/\chi^l_{\nu_0}) ,$$

where $\chi^c_\nu$ is the continuous opacity at $\nu$ and $\chi^l_{\nu_0}$ the line opacity at line center, $S^c_\nu$ is the continuum source function, and $S^l_\nu$ is the line source function. In CRD, $S^l_\nu$ is defined by

$$S^l_\nu = \frac{\bar{J} + \epsilon B^s}{1 + \epsilon} , \quad (2)$$

$$\bar{J} = \int_0^\infty \phi_\nu J_\nu \, d\nu , \quad (3)$$

$$\epsilon = (R_d - \beta R_p)/A_{ji} , \quad (4)$$

$$B^s = B_\nu[R_p(1 - \beta)/(R_d - \beta R_p)] , \quad (5)$$

where $\phi_\nu$ is given by the Voigt function, with the damping constants given by Appendix A of Vernazza, Avrett, and Loeser (1981); $\beta = \exp(-h\nu/kT)$; $R_p$ is the photon production rate; and $R_d$ is the photon destruction rate. $S^l_\nu$ becomes equal to $B_\nu(T_e)$ when $\epsilon \gg 1$ (e.g., when the collisional rates dominate) or at large optical depths where $J_\nu = B^s = B_\nu$.

The continuous opacities used in the calculation of $r_\nu$ and $S^c_\nu$ include those of bound-free and free-free $H^-$ and $H_2^+$; free-free H I, He I, He II, and $He^-$; electron scattering; H I Rayleigh scattering; and the bound-free opacities of H I, He I, He II, C I, Mg I, Al I, Si I, and Fe I as calculated by equations (1), (2a), and (2b) of Vernazza, Avrett, and Loeser (1976) and Table 16 of Vernazza, Avrett, and Loeser (1981). Recently the bound-free opacities of Na I and Ca I have been added to PANDORA. They have the same functional form as the opacities above, with the threshold cross section ($\sigma_{th}$), threshold ionization wavelength ($\lambda_l$), statistical weight ($g_l$), and spectral index ($s_l$) listed in Table 2. The Na I 3*s* data were obtained experimentally by Hudson and Carter (1967), the 3*p* data were obtained by Rothe (1969), the 4*s* and 4*p* data are taken from the calculations of Aymar (1978) and Aymar, Luc-Koenig, and Combet Farnoux (1976), and the 2*d* terms were calculated by Peach (1970). The Ca I 4*s* data were taken from Scott, Kingston, and Hibbert (1983); the other levels are taken from Kelm and Schluter (1962) and Ayres and Testerman (1978). Rayleigh scattering by the $H_2$ molecule and He atoms are important opacity sources in these cool stars and have been added as well. For $H_2$ Rayleigh scattering, tabulated cross sections from Victor and Dalgarno (1969) are used for $\lambda > 6328$ Å, and a polynomial expression for the cross section is used for 1200 Å $\leq \lambda \leq$ 6328 Å (Tarafdar and Vardya 1973). For He I Rayleigh scattering, tabulated cross sections (Langhoff, Sims, and Corcoran 1974) are used for $\lambda > 9227$ Å, and a polynomial expression for the cross section is used for 920 Å $\leq \lambda \leq$ 9227 Å (Baschek and Scholz 1982).

Chromospheric emission in the Mg II resonance lines is severely mutilated by the circumstellar absorption lines of Mn I at 2794.82 Å and Fe I at 2795.01 and 2803.16 Å. Another Mn I line lies at 2801.08 Å, but its influence on the Mg II *h* line should be minimal, since it lies 1.6 Å from line center and 1.0 Å from the *h* blue-wing emission peak. Eriksson *et al.* (1986) speculate on possible circumstellar absorption from the molecules SiO, CS, and SiS, but no direct evidence for these

TABLE 2A

BOUND-FREE OPACITY DATA

| Level | $\sigma_{th}$ ($10^{-18}$ cm$^2$) | $\lambda_l$ (Å) | $g_l$ | $s_l$ |
|---|---|---|---|---|
| **Na I** | | | | |
| $3s\ ^2S_{1/2}$ | 0.129[a] | 2413 | 2 | 1 |
| $3p\ ^2P_{1/2}$ | 7.93 | 4083 | 2 | 4 |
| $3p\ ^2P_{3/2}$ | 7.93 | 4086 | 4 | 4 |
| $4s\ ^2S_{1/2}$ | 0.803 | 6366 | 2 | 3 |
| $3d\ ^2D_{5/2}$ | 3.61 | 8148 | 6 | 3 |
| $3d\ ^2D_{3/2}$ | 3.61 | 8149 | 4 | 3 |
| $4p\ ^2P_{1/2}$ | 18.71 | 8943 | 2 | 3 |
| $4p\ ^2P_{3/2}$ | 18.71 | 8948 | 4 | 3 |
| **Ca I** | | | | |
| $4s\ ^1S_0$ | 1.0[b] | 2028 | 1 | 0 |
| $4p\ ^3P^o_{3/2}$ | 6.1 | 2933 | 3 | 21 |
| $4p\ ^3P^o_{5/2}$ | 12.2 | 2940 | 6 | 21 |
| $3d\ ^3D_{2,1,0}$ | 5.0 | 3435 | 15 | 14 |
| $3d\ ^1D_2$ | 10.3 | 3643 | 5 | 3 |
| $4p\ ^1P^o_1$ | 7.49 | 3899 | 3 | 2 |
| $5s\ ^3S_1$ | 2.86 | 5629 | 3 | 3 |
| $4p\ ^1P^o_1$ | 2.2 | 7953 | 3 | 3 |

[a] The $3s\ ^2S_{1/2}$ level is multiplied by $f(\lambda)$ interpolated from Table 2B; $f(\lambda) = 0$ for $\lambda < 800$ Å and $\lambda > 2413$ Å.

[b] The $4s\ ^1S_0$ level is multiplied by $f(\lambda)$ interpolated from Table 2B; $f(\lambda) = 0$ when $\lambda < 912$ Å and $\lambda > 2028$ Å.

TABLE 2B

GROUND-STATE INTERPOLATION TABLE FOR $f(\lambda)$

| $\lambda$ (Å) | $f(\lambda)$ | $\lambda$ (Å) | $f(\lambda)$ | $\lambda$ (Å) | $f(\lambda)$ |
|---|---|---|---|---|---|
| *a)* Na I $3s\ ^2S_{1/2}$ Level | | | | | |
| 2413 | 1.0 | 1950 | 0.018 | 1400 | 0.9 |
| 2300 | 0.71 | 1800 | 0.057 | 1200 | 1.22 |
| 2200 | 0.36 | 1700 | 0.29 | 1000 | 1.32 |
| 2100 | 0.083 | 1600 | 0.54 | 800 | 1.4 |
| *b)* Ca I $4s\ ^1S_0$ | | | | | |
| 2028 | 1.26 | 1900 | 4.80 | 1780 | 0.60 |
| 2020 | 1.09 | 1890 | 190 | 1770 | 0.80 |
| 2010 | 0.87 | 1885 | 235 | 1760 | 0.80 |
| 2000 | 0.68 | 1880 | 180 | 1750 | 0.80 |
| 1990 | 0.50 | 1870 | 7.30 | 1700 | 0.73 |
| 1980 | 0.33 | 1860 | 4.00 | 1650 | 0.67 |
| 1970 | 0.20 | 1850 | 2.50 | 1600 | 0.61 |
| 1960 | 0.10 | 1840 | 1.80 | 1500 | 0.50 |
| 1950 | 0.04 | 1830 | 1.20 | 1400 | 0.40 |
| 1940 | 0.04 | 1820 | 1.00 | 1300 | 0.32 |
| 1930 | 0.10 | 1810 | 0.80 | 1100 | 0.19 |
| 1920 | 0.80 | 1800 | 0.60 | 912 | 0.15 |
| 1910 | 2.00 | 1790 | 0.50 | | |

absorbers over the Mg II lines can be seen. For this study we assume that the blue wing of the Mg II *h* line is unaffected by circumstellar (and interstellar) absorption and use it as the primary chromospheric-structure indicator.

We initially had difficulty in producing Mg II *h* and *k* lines in emission due to their high $A_{ji}$ values and the low density of our model. A very steep temperature gradient in the lower chromosphere is required to produce the observed emission. In addition, the bound-free opacity from Ca I ($4p\,^3P^o$) is required to reduce the continuum near Mg II *h* and *k* to observed values.

Figure 1 shows the final CRD flux calculation for Mg II *h* and *k* compared with the high-resolution *IUE* spectrum of TX Psc. The synthetic profiles are convolved with a Gaussian with the *IUE* FWHM at 2800 Å of 0.2 Å (*IUE/NASA Newsletter*, No. 28, 1985 November) and scaled to the angular diameter of TX Psc. From the figure it is obvious that the line wings have much more flux than the observations, and no chromospheric temperature-density profile could be found to overcome this discrepancy. The only mechanisms that will reduce these rings are an increase of continuous absorption at higher layers in the photosphere or the inclusion of PRD in the source function calculations.

The integrated flux of the C II] (UV 0.01) multiplet for this model ($7.7 \times 10^{-13}$ ergs s$^{-1}$ cm$^{-2}$) is $\sim$2.7 times the observed flux of the two low-resolution *IUE* spectra that bracket the high-resolution spectrum. These lines are formed at the same depth as the Mg II *h* and *k* emission peaks. Because of their lower oscillator strengths, C II] (UV 0.01) is more closely coupled to the Planck function than Mg II *h* and *k*, and this CRD model cannot be the correct one for TX Psc.

### b) *Partial Redistribution in a Static Atmosphere*

Because the low densities in this model atmosphere allow line-scattering processes to dominate pure absorption processes, a proper treatment of the redistribution of scattered photons must be incorporated. We follow the PRD description of Avrett and Loeser (1984). The line source function in PRD is described by

$$S_\nu^l = \frac{1}{1+\epsilon}\left[\frac{1}{\phi_\nu}\int R(\nu', \nu) J_{\nu'}\, d\nu' + \epsilon B^s\right]. \quad (6)$$

The redistribution function $R(\nu', \nu)$ is assumed to be a combination of coherent scattering and complete redistribution, corresponding to the first and second terms, respectively, in the equation

$$R(\nu', \nu) = \gamma_s \langle a\rangle_\nu \phi_{\nu'}\, \delta(\nu - \nu') + (1 - \gamma_s a_{\nu',\nu})\phi_{\nu'}\phi_\nu\,, \quad (7)$$

where

$$\gamma_s = \Gamma_{\rm rad}/\Gamma_{\rm total}\,, \quad (8)$$

$$\langle a\rangle_\nu = \int a_{\nu',\nu}\,\phi_{\nu'}\, d\nu'\,, \quad (9)$$

$$a_{\nu',\nu} = f(x) = \begin{cases} 0\,, & x \le x_c\,, \\ 1 - \exp\{-[(x - x_c)/x_c]^2\}\,, & x > x_c\,, \end{cases} \quad (10)$$

and

$$x = \max\left(\frac{|\nu - \nu_0|}{\Delta\nu_{\rm D}}, \frac{|\nu' - \nu_0|}{\Delta\nu_{\rm D}}\right). \quad (11)$$

In the above equations, $\Gamma_{\rm total}$ is the sum of the collisional ($\Gamma_{\rm coll}$) and radiative ($\Gamma_{\rm rad}$) damping coefficients (Appendix A of Vernazza, Avrett, and Loeser 1981), $\Delta\nu_{\rm D}$ is the Doppler width, and $\nu$ and $\nu'$ are frequencies of emission and absorption in the observer's frame, respectively. The parameter $x_c$ in equation (10) is the critical displacement in Doppler units separating the CRD–dominated line core and the coherent scattering–

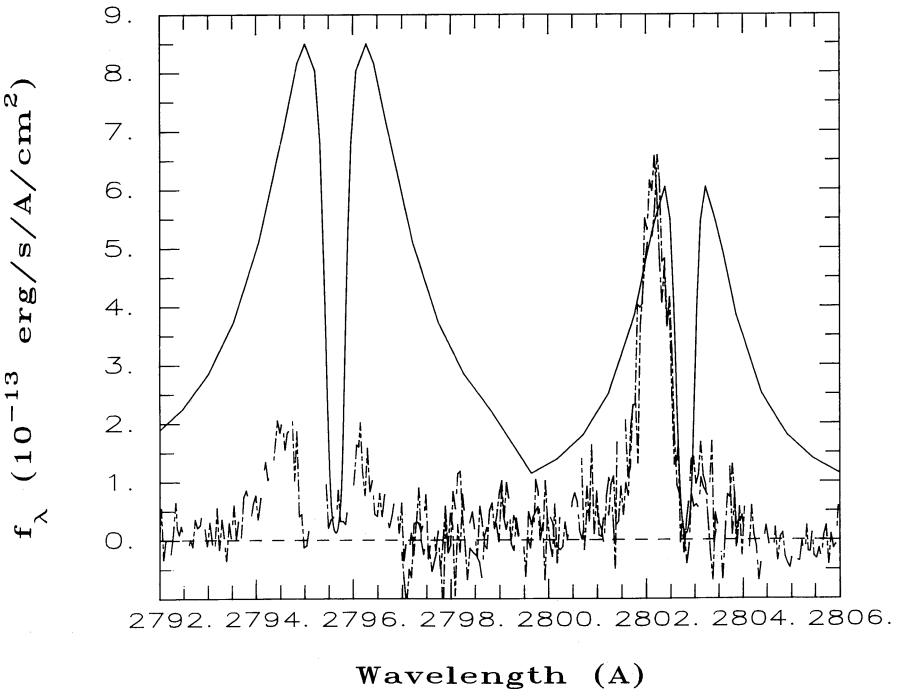


FIG. 1.—Comparison of our best CRD static atmosphere Mg II *k* and *h* synthetic flux calculation (*solid line*) and the high-resolution *IUE* spectrum of TX Psc (*dashed line*). Note that the line wings are too strong compared with the *IUE* spectrum. The synthetic spectrum has been convolved with a Gaussian of 0.2Å FWHM (*IUE/NASA Newsletter*, No. 28, 1985 November) and shifted by the radial velocity of TX Psc (+12 km s$^{-1}$).

dominated line wings. This parameter is assumed constant at all depths in this approximation of PRD. We tested a variety of values for $x_c$. The Mg II emission cores were much too narrow for $x_c = 2$, and no modification in the temperature-density stratification could be made to reproduce the width of the emission features. The best fit to the observed broadening of the emission core was obtained for $x_c = 6$.

This partial coherent scattering (PCS) approximation for the redistribution function $R(\nu', \nu)$ in equation (7) has been criticized because it does not account for Doppler diffusion of photons in the line wings (Basri 1980; Frisch 1980). Hubený (1985) has recently presented a new approximate numerical method for solving PRD transfer problems. Hubený uses the PCS approximation and shows that photon diffusion in the line wings can be accounted for in a simple manner by allowing $x_c$ to vary with depth in the atmosphere, where $x_c$ is a function of the Voigt parameter $a$ and the *mean optical depth* for the line. Using the formalism of Hubený, $x_c$ lies between 5 and 7 over the depths of formation of the Mg II emission features. Although the line profile is sensitive to the value of $x_c$ in the approximation used in this study, the empirical value of $x_c = 6$ should mimic the Hubený formalism at the depth of formation of the Mg II emission features.

Photons absorbed in the line core cannot escape as easily in the wings for our PRD approximation as compared with the CRD approximation. As such, these photons are trapped in the line core, which results in an increased flux of the Mg II emission profiles for the given chromospheric model. This requires a decrease in the electron temperature in the layers where the Mg II emission profiles are formed. Figure 2 shows the resulting "best fit" of the synthetic spectrum in PRD as compared with the high-resolution *IUE* spectrum. The synthetic spectrum has been shifted by the radial velocity of TX Psc ($+12$ km s$^{-1}$). Except for the velocity shifts of the emission features, the calculated blue wing of the $h$ line now resembles the *IUE* spectrum quite well and demonstrates the accuracy both of the method and the chromospheric model. The lower temperatures in the layers where the Mg II emission originates also produce C II] (UV 0.01) integrated line fluxes of $2.5 \times 10^{-13}$ ergs s$^{-1}$ cm$^{-2}$ ($\sim 0.9 f_{\rm obs}$). Figure 3 displays the temperature as a function of height for this PRD model and compares it with the CRD model.

### c) *Partial Redistribution in an Expanding Atmosphere*

Mg II $h$ is less affected than the $k$ line by circumstellar absorption and as such displays the velocity blueshift of the emission wings with greater clarity. Figures 1 and 2 show that the self-absorption (or perhaps interstellar absorption) portion of Mg II $h$ is at rest with respect to the radial velocity of the star. The noise in the high-resolution *IUE* spectrum and the large amount of *circumstellar* absorption overlying the Mg II $h$ and $k$ lines prevent the identification of the interstellar absorption features. We assume that most of the *zero-velocity* absorption is due to self-absorption of Mg II in the outer layers of the stellar atmosphere. Since this portion of the line comes from the upper chromosphere, these layers are stationary with respect to the photosphere. The emission portion of the line originates in the lower chromosphere where $S_\nu$ reaches a local maximum. In this region, we initially introduce a velocity field with $v_{\rm max}$ occurring where $dS_\nu/dh = 0$ in the chromosphere. For the layers below this region, we follow the continuity equation $\rho v r^2 = \rho_0 v_0 r_0^2$, where $v_0 = v_{\rm max}$, and for layers above this region we force the velocity to a low value at the top of the chromosphere ($\sim 1$ km s$^{-1}$), since the continuity equation gives unrealistic velocities because of the low density in these regions.

The method used in solving the radiative transfer equation for PRD in an expanding atmosphere is described in detail by

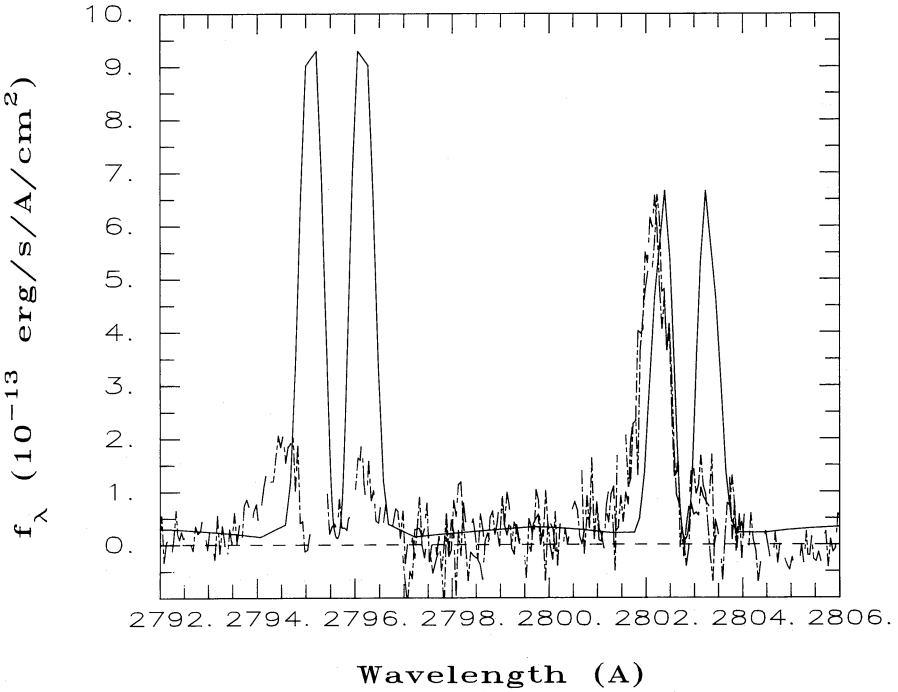


FIG. 2.—Comparison of our best PRD static atmosphere flux calculation (*solid line*) to the observed high-resolution spectrum of Mg II $k$ and $h$ (*dashed line*). As in Fig. 1, the synthetic spectrum has been convolved with the instrumental profile and shifted by $+12$ km s$^{-1}$.

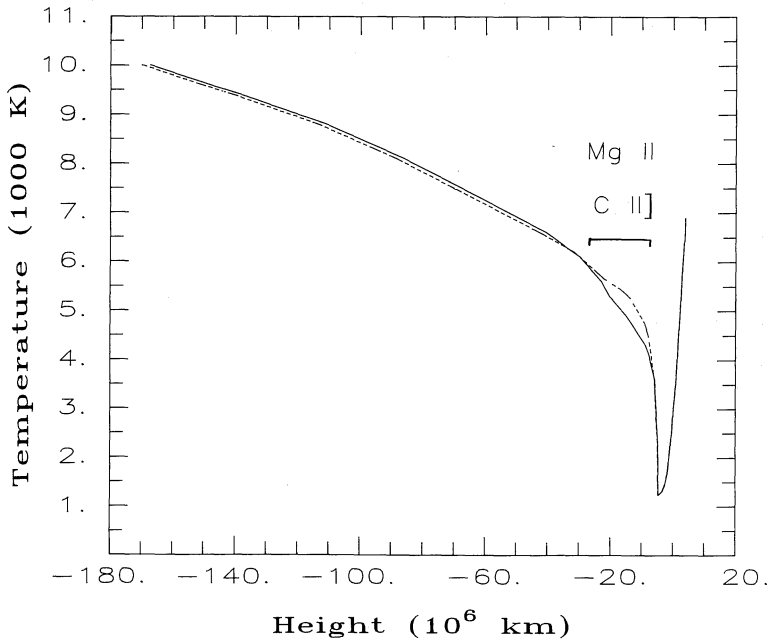


FIG. 3.—Temperature as a function of height for the CRD model (*dashed line*) and the PRD model (*solid line*). The location in the atmosphere where the Mg II and C II] emission features are formed is indicated.

Avrett and Loeser (1984). A variety of values of $v_{max}$ were tested to reproduce the *h* line. In these calculations, the assumption of detailed balance in the Lyman lines is relaxed, resulting in a change to the final chromospheric structure as described in § IV. The maximum chromospheric expansion velocity was found by the best fit to be near 50 km $s^{-1}$ at depth $z = -5.9 \times 10^6$ km ($3.2 \times 10^6$ km below the region where $dS_\nu/dh = 0$). However, the base of the Mg II *h* and *k* emission features is not broad enough, and an increase in the microturbulent velocity from 5 to 7 km $s^{-1}$ near the temperature minimum region is needed to reproduce the observations. The chromospheric structure deduced from this Mg II calculation now produces C II] (UV 0.01) flux that matches the observations ($3.2 \times 10^{-13}$ ergs $s^{-1}$ $cm^{-2}$). Figure 4 displays the

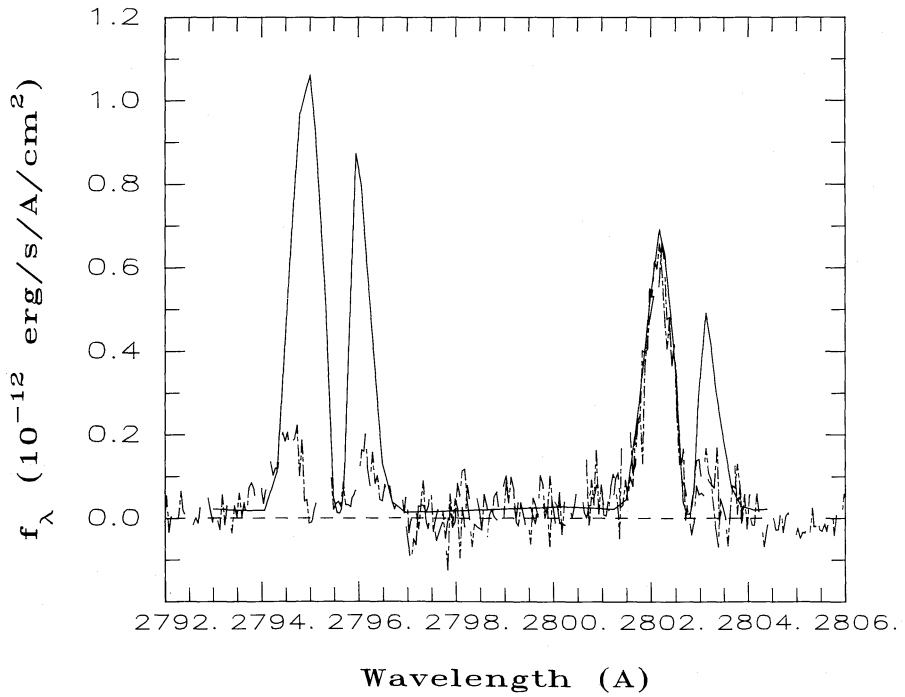


FIG. 4.—Comparison of our best PRD expanding chromosphere flux calculation (*solid line*), convolved and shifted, to the high-resolution *IUE* spectrum (*dashed line*).

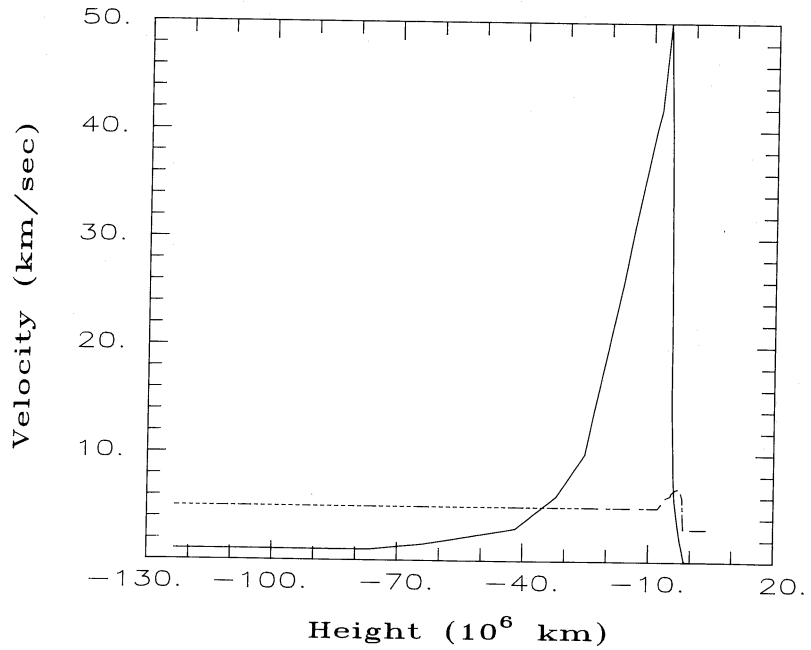


FIG. 5.—Resulting expansion velocity field (*solid line*) and the microturbulent velocity (*dashed line*) of the PRD expanding chromosphere calculation. The synthetic flux calculated with this velocity field is displayed in Fig. 4.

resulting flux for the Mg II doublet calculated with the PRD model, and Figure 5 shows the expansion velocity and the microturbulent velocity.

The large amount of circumstellar absorption over the Mg II lines makes it difficult to separate Mg II interstellar absorption and Mg II self-absorption from the upper chromosphere. We *assume* that most of the absorption over the Mg II lines at zero velocity (stellar frame) is due to self-absorption from the upper chromosphere. We now examine possible effects of interstellar absorption on the Mg II emission.

Using the Bohlin, Savage, and Drake (1978) expression for the relation between interstellar hydrogen column density and interstellar reddening, $n_H/E(B-V) = 5.8 \times 10^{21}$ atoms cm$^{-2}$ mag$^{-1}$, and assuming various values for velocity and reddening of the ISM between Earth and TX Psc, we investigated the effect of interstellar absorption over the Mg II lines. Walker (1980) reports $E(B-V) = 0$ for TX Psc, which leads to no interstellar absorption. Nevertheless, to investigate any possible effects, we first assumed $E(B-V) = 0.0002$, and we let the velocity dispersion ($v_{disp}$) of the interstellar lines vary from 1 to 10 km s$^{-1}$, and the radial velocity ($v_{rad}$) of the ISM lines vary from $-30$ km s$^{-1}$ to $+50$ km s$^{-1}$. To set an upper limit on the Mg II abundance, we also assumed that the ISM has a solar composition and that all the magnesium is singly ionized. No interstellar feature was obvious on the synthetic spectrum for $E(B-V) = 0.0002$ at any velocity. To set an upper limit on the amount of interstellar absorption over the Mg II lines, we then set $E(B-V) = 0.02$ for TX Psc. For $v_{disp} < 2$ km s$^{-1}$, the lines were not detectable at any $v_{rad}$, owing to the convolution of the synthetic flux. A distinct interstellar feature could be seen for $v_{disp} > 5$ km s$^{-1}$ and $v_{rad} > +35$ km s$^{-1}$ and $v_{rad} < -18$ km s$^{-1}$. We can eliminate radial velocities less than $-5$ km s$^{-1}$ for the ISM, since evidence for this velocity range would show up in the short-wavelength side of the *h* line emission feature. Since the short-wavelength side of the *h* line is the primary feature used in our semiempirical model and interstellar absorption does not affect this feature, we believe our model to be valid for TX Psc with the assumptions used.

With this final spectrum, we can calculate the intrinsic chromospheric flux of the Mg II resonance lines and compare it with the observed flux and with M giant Mg II fluxes. The scaled synthetic flux gives $1.3 \times 10^{-12}$ ergs cm$^{-2}$ s$^{-1}$ for the *k* line, $7.6 \times 10^{-13}$ ergs cm$^{-2}$ s$^{-1}$ for the *h* line, and a total scaled flux of $2.0 \times 20^{-12}$ ergs cm$^{-2}$ s$^{-1}$ for Mg II. In comparison with the observations, $f(k)_{intrinsic} \simeq 5.4 f(k)_{obs}$, $f(h)_{intrinsic} \simeq 1.8 f(h)_{obs}$, and $f(\text{Mg II})_{intrinsic} \simeq 3.0 f(\text{Mg II})_{obs}$. The calculated Mg II chromospheric flux is still one-third of the observed Mg II chromospheric flux for RZ Ari (M6 III) when both fluxes are normalized by their respective bolometric fluxes (Johnson and Luttermoser 1987). This indicates that the circumstellar absorption may not be the sole cause of the low Mg II fluxes seen in the low-resolution *IUE* spectra of N-type carbon stars; the chromospheres of these stars must be cooler (assuming that the blue wing of the Mg II *h* line is not affected by circumstellar absorption) than early and middle M-type stars (i.e., M0–M6).

## IV. OTHER SPECTRAL FEATURES

As stated earlier, resonance lines of neutral metals are not seen in emission in the LWP low-resolution *IUE* spectra of N-type stars. Mg I has sufficient opacity in this chromospheric model to form an emission peak in the line core. However, the flux in this emission core is too low ($\sim$54% of the continuum flux) to be recorded by either the high- or the low-resolution cameras aboard *IUE*. In addition, circumstellar (and possibly interstellar) absorption would reduce the flux of this emission peak to even lower values. Eaton and Johnson (1988) have noted Mg I $\lambda$2852 in emission for middle M-type stars, so the emission seen in our calculations is not a problem—as long as it is not too great.

The Ca II H and K lines are also calculated in non–LTE and PRD to see whether the calculations could produce lines with no emission bumps. The calculations give rise to some emis-

sion features (~32% of the continuum flux for the K line), and convolving these lines with an instrument profile of 1 Å FWHM still produced emission features which should be seen. However, like the Mg II *h* and *k* emission peaks, circumstellar (and possibly interstellar) absorption may reduce the flux of the Ca II H and K emission peaks. Atomic lines which should have significant opacity in the circumstellar shell at the wavelengths of the Ca II emission peaks (shifted by +50 km $s^{-1}$) include Sc I λ3933.4; Ti I λ3934.2; V I λλ3932.7, 3933.5, 3934.0; Fe I λλ3932.6, 3969.3; Co I λλ3933.9, 3968.6; and Zr I λλ3966.7, 3968.3. This suspected amount of circumstellar absorption along with the convolution of the instrument profile should easily hide these weak emission features.

Balmer lines are also not seen. The line-center flux of Hα from the 3 level model atom with the PRD temperature profile is 21% of the continuum flux level and has a FWHM of 0.6 Å. This is a respectable line strength which should easily be seen. However, many CN lines fall within this wavelength region, which obliterates the "true" continuum in the emergent spectrum. The average emergent flux level for 6540 Å < λ < 6585 Å with atomic and molecular lines included in LTE flux calculations is ~8% with respect to the continuum flux. Thus, Hα would not be very apparent in this "CN forest," although there may still be a residual problem, since Hα is generally not seen at all in these stars.

We now compare the results obtained from our three hydrogen atomic models: (1) the simplified 3 level case, (2) the full 3 level atom, and (3) the 4 level atom. We first relax the assumption of detailed balance in Lyα and Lyβ and the assumption of $J_\nu = WB_\nu(T_{\rm rad})$ in the Balmer and Paschen continua in the 3 level atom. The line-center flux of Hα with the PRD model is now 86% of the continuum flux with a FWHM of 0.4 Å; this would be very difficult to detect among the CN lines in this portion of the spectrum. The number density in the second level of hydrogen is decreased by 3 orders of magnitude in the middle chromosphere and 1 order of magnitude in the lower chromosphere with the relaxation of the above-mentioned assumptions in the 3 level atom. Although the Lyman lines are optically thick throughout most of the chromosphere, the net radiative rate, $A_{ji}\rho_{ji}$, where $A_{ji}$ is the Einstein *A*-value and $\rho_{ji}$ the net radiative bracket, is larger than the collisional rates $C_{ji}$ [e.g., $A_{21}\rho_{21} = 13.6$ and $C_{21} = 7.5 \times 10^{-3}$ in the middle chromosphere ($z = -2.5 \times 10^7$ km) and $A_{21}\rho_{21} = 3.4$ and $C_{21} = 0.4$ in the lower chromosphere ($z = -7.79 \times 10^6$ km)]. As a result, the assumption $\rho_{ji} = 0$ in the Lyman lines is not valid, hence detailed balancing does not hold for these lines *in the chromosphere*. Relaxing detailed balancing in Lyα and Lyβ allows electrons in the second and third levels to cascade down to the first level and reduces the densities in levels 2 and 3. The calculated photoionization radiation temperature of level 2 is 2700 K, and that of level 3 is 2450 K, in this chromospheric model.

Another result from the relaxation of the detailed-balance assumption in the Lyman lines is a decrease in a hydrogen ionization. Hydrogen is underionized, with respect to the calculations made assuming detailed balance in Lyα and Lyβ, by a factor of 100 in the lower chromosphere. This results in a decrease of electron density by a factor of 10 in the middle chromosphere and a factor of 1.6 in the region of the chromosphere where Mg II (UV 1) and C II] (UV 0.01) are formed. As a result, the temperature profile in this region is increased by ~400 K (cf. § IIIc) to bring the synthetic flux back to the observed values. The ionization equilibrium of this model will be investigated in a future paper.

In comparison with the solution of the full 3 level case, using a 4 level H atom produces little change in the level, ion, and electron densities and the Hα line profile. As a result, we do not expect additional levels to influence these results drastically.

## V. CONCLUSIONS

We construct a semiempirical chromospheric model of TX Psc based on the Mg II *h* and *k* line profiles, C II] (UV 0.01) integrated line flux, Mg I, and overall appearance of the low-resolution, long-wavelength *IUE* region and the Hα spectral region. Table 3 lists the atmospheric parameters that describe the model. Using the continuous opacities presented earlier and the assumptions that the chromospheric temperature increases monotonically and that a depth-independent PCS formalization mimics PRD in the radiation field of this star, we have determined a constrained chromospheric model for TX Psc. The outermost layers of this model are the most uncertain, because of the lack of spectral indicators formed in this region. The temperatures and densities in the outermost layers are constrained to allow the optical depth of Mg II *h* and *k* and the C II resonance lines to be small at the top of the atmosphere.

Johnson, Luttermoser, and Faulkner (1988) have demonstrated the great influence of neutral metal lines in the spectra of these cool stars, especially in the ultraviolet and violet. We have included background continuum opacity multipliers based on the opacities of the LTE flux calculations of Johnson, Luttermoser, and Faulkner (1988) to simulate the effect of the multitude of atomic and molecular lines on the line profiles of C II] (UV 0.01), Mg II (UV 1), Mg I (UV 1), Ca II (1), and Hα. Although this additional opacity affects the wings of the resonance lines and causes Hα to become virtually nonexistent, it has little or no effect on the emission peaks of the above-mentioned resonance lines and no effect on C II.

We conclude the following from this study. (1) The chromospheric temperature rise must begin at a sufficiently low density [in this model $\rho(T_{\rm min}) = 6.6 \times 10^{-12}$ g $cm^{-3}$] to (*a*) ensure that strong neutral metal lines (especially Mg I λ2852) are so optically thin as to be weakly affected by the chromospheric temperature rise (although it may be possible to hide weak emission with circumstellar and possibly interstellar absorption), (*b*) prevent Balmer lines from becoming too strong, and (*c*) allow semiforbidden lines like C II] and Al II] to form. (2) The temperature gradient in the lower chromosphere must be high (a rise of 3600 K over three pressure scale heights—the extent of the lower chromosphere) to produce the required emission in Mg II *h* and *k* and C II] (UV 0.01). (3) Ca I ($4p\,^3P^o$) bound-free opacity must be included in the Mg II *h* and *k* calculations to reproduce the continuum level in this spectral region. (4) Partial redistribution effects in the resonance lines are very strong and must be used in the Mg II *h* and *k* calculations. (5) The lower chromosphere is expanding away from the photosphere with a velocity near 50 km $s^{-1}$, but the upper chromosphere is nearly static with respect to the photosphere. (6) The microturbulent velocity is 7 km $s^{-1}$ at the temperature minimum region and drops quickly to 5 km $s^{-1}$ in the chromosphere. (7) Finally, even though the Lyman lines are optically thick in most of the chromosphere, the collisional rates are so small that these lines are not in detailed balance in the chromosphere.

What type of heating mechanism might exist in TX Psc to produce such a chromospheric model? Short-period waves ($P < 1$ day) cannot be responsible, since the Mg II flux in TX Psc is fairly constant in the high-resolution *IUE* spectrum and the two low-resolution *IUE* spectra that bracket the high-

TABLE 3

MODEL ATMOSPHERE FOR TX PISCIUM

| Height (km) | Temp (K) | Column Mass (gm/cm$^3$) | Total Pressure (dyne/cm$^3$) | Hydrogen Density (/cm$^3$) | Electron Density (/cm$^3$) | Proton Density (/cm$^3$) |
|---|---|---|---|---|---|---|
| -1.23E+08 | 10000. | 8.10E-12 | 8.10E-12 | 4.26E+00 | 1.18E+00 | 7.47E-01 |
| -1.12E+08 | 9600. | 3.50E-11 | 3.50E-11 | 2.08E+01 | 3.50E+00 | 1.37E+00 |
| -1.06E+08 | 9400. | 8.00E-11 | 8.00E-11 | 4.98E+01 | 6.81E+00 | 1.73E+00 |
| -9.12E+07 | 8800. | 8.10E-10 | 8.10E-10 | 5.53E+02 | 5.87E+01 | 2.31E+00 |
| -8.13E+07 | 8300. | 4.20E-09 | 4.20E-09 | 3.05E+03 | 3.13E+02 | 2.54E+00 |
| -7.70E+07 | 8100. | 8.80E-09 | 8.80E-09 | 6.54E+03 | 6.70E+02 | 2.72E+00 |
| -6.41E+07 | 7500. | 9.00E-08 | 9.00E-08 | 7.25E+04 | 7.14E+03 | 4.67E+00 |
| -4.17E+07 | 6600. | 9.90E-06 | 9.90E-06 | 9.84E+06 | 4.02E+04 | 5.23E+02 |
| -3.21E+07 | 6250. | 1.00E-04 | 1.00E-04 | 1.05E+08 | 1.80E+05 | 3.23E+03 |
| -2.53E+07 | 6050. | 5.50E-04 | 5.50E-04 | 5.98E+08 | 8.41E+05 | 9.23E+03 |
| -2.26E+07 | 5950. | 1.10E-03 | 1.10E-03 | 1.22E+09 | 1.59E+06 | 1.27E+04 |
| -1.65E+07 | 5700. | 5.60E-03 | 5.60E-03 | 6.46E+09 | 7.34E+06 | 2.21E+04 |
| -1.40E+07 | 5550. | 1.10E-02 | 1.10E-02 | 1.30E+10 | 1.40E+07 | 2.41E+04 |
| -9.11E+06 | 5100. | 4.50E-02 | 4.50E-02 | 5.81E+10 | 3.25E+07 | 2.26E+04 |
| -7.84E+06 | 4700. | 6.70E-02 | 6.70E-02 | 9.38E+10 | 2.06E+07 | 1.93E+04 |
| -5.86E+06 | 3600. | 1.40E-01 | 1.40E-01 | 2.56E+11 | 2.91E+07 | 2.34E+03 |
| -5.22E+06 | 2800. | 1.90E-01 | 1.90E-01 | 4.47E+11 | 1.60E+07 | 3.34E+01 |
| -4.78E+06 | 2200. | 2.50E-01 | 2.50E-01 | 7.53E+11 | 1.12E+07 | 6.38E-03 |
| -4.72E+06 | 1600. | 2.70E-01 | 2.70E-01 | 1.94E+12 | 1.78E+07 | 8.35E-05 |
| -4.68E+06 | 1239. | 2.90E-01 | 2.90E-01 | 2.82E+12 | 2.05E+07 | 3.74E-07 |
| -4.45E+06 | 1245. | 4.90E-01 | 4.90E-01 | 4.75E+12 | 2.76E+07 | 1.77E-09 |
| -4.20E+06 | 1260. | 8.60E-01 | 8.60E-01 | 8.24E+12 | 3.84E+07 | 1.63E-09 |
| -3.89E+06 | 1276. | 1.70E+00 | 1.70E+00 | 1.61E+13 | 5.97E+07 | 1.50E-09 |
| -3.37E+06 | 1310. | 5.40E+00 | 5.40E+00 | 4.98E+13 | 1.38E+08 | 1.02E-09 |
| -2.57E+06 | 1430. | 2.80E+01 | 2.80E+01 | 2.36E+14 | 5.15E+08 | 4.96E-09 |
| -1.95E+06 | 1610. | 8.90E+01 | 8.90E+01 | 6.65E+14 | 1.36E+09 | 5.94E-08 |
| -1.78E+06 | 1680. | 1.20E+02 | 1.20E+02 | 8.58E+14 | 1.72E+09 | 1.63E-07 |
| -1.60E+06 | 1755. | 1.60E+02 | 1.60E+02 | 1.09E+15 | 2.16E+09 | 5.38E-07 |
| -1.40E+06 | 1870. | 2.20E+02 | 2.20E+02 | 1.39E+15 | 2.79E+09 | 3.35E-06 |
| -1.23E+06 | 1980. | 2.80E+02 | 2.80E+02 | 1.64E+15 | 3.40E+09 | 4.56E-05 |
| -1.02E+06 | 2100. | 3.70E+02 | 3.70E+02 | 1.98E+15 | 4.36E+09 | 2.76E-04 |
| -9.14E+05 | 2150. | 4.20E+02 | 4.20E+02 | 2.15E+15 | 4.93E+09 | 1.29E-03 |
| -6.82E+05 | 2350. | 5.40E+02 | 5.40E+02 | 2.24E+15 | 6.26E+09 | 1.40E-02 |
| -5.51E+05 | 2420. | 6.10E+02 | 6.10E+02 | 2.33E+15 | 7.13E+09 | 4.93E-02 |
| -2.71E+05 | 2550. | 7.70E+02 | 7.70E+02 | 2.53E+15 | 9.39E+09 | 6.98E-01 |
| -7.64E+04 | 2780. | 8.80E+02 | 8.80E+02 | 2.28E+15 | 1.13E+10 | 4.06E+01 |
| 1.50E+05 | 2990. | 1.00E+03 | 1.00E+03 | 2.27E+15 | 1.59E+10 | 1.05E+03 |
| 6.75E+05 | 3310. | 1.30E+03 | 1.30E+03 | 2.60E+15 | 3.80E+10 | 7.97E+04 |
| 1.29E+06 | 3860. | 1.70E+03 | 1.70E+03 | 2.90E+15 | 1.53E+11 | 2.12E+07 |
| 1.73E+06 | 4390. | 2.00E+03 | 2.00E+03 | 3.00E+15 | 3.13E+11 | 1.68E+09 |
| 2.01E+06 | 4700. | 2.20E+03 | 2.20E+03 | 3.08E+15 | 3.92E+11 | 1.60E+10 |
| 2.54E+06 | 5200. | 2.60E+03 | 2.60E+03 | 3.29E+15 | 7.39E+11 | 2.62E+11 |
| 3.06E+06 | 5900. | 3.00E+03 | 3.00E+03 | 3.34E+15 | 3.30E+12 | 2.60E+12 |
| 3.79E+06 | 6600. | 3.60E+03 | 3.60E+03 | 3.58E+15 | 1.43E+13 | 1.31E+13 |
| 3.91E+06 | 6900. | 3.70E+03 | 3.70E+03 | 3.51E+15 | 2.43E+13 | 2.29E+13 |

resolution spectrum (see Table 1). Alfvén waves do not seem likely, since TX Psc is large and thus rotates slowly. Hartmann and Avrett (1984) have generated models for the extended chromosphere of $\alpha$ Ori based on Alfvén wave heating. To reproduce the mass-loss rate of $\alpha$ Ori, they deduced a surface magnetic field of 2 G (although their model has trouble in reproducing the chromospheric line profiles of Mg II *h* and *k* and Ca II H and K). It is hard to image how dynamos in extremely slowly rotating supergiants (like TX Psc) could produce fields this large.

Long-period waves would appear to be the best mechanism for heating the outer atmospheres of carbon stars. Variability in the Mg II lines of TX Psc at least on the order of 62 days has been documented (Johnson *et al.* 1986). This study has shown that circumstellar obscuration may not be entirely responsible for this variation, and the velocity field deduced from the Mg II lines indicates the existence of supersonic flows in the emitting regions (the isothermal sound speed is $\sim 10$ km s$^{-1}$ where the expansion velocity is at a maximum [$\sim 50$ km s$^{-1}$]). Some type of acoustic shock mechanism is probably responsible for the emission lines seen in the *IUE* spectra of this star, as is the case in Mira-type variables (Brugel, Willson, and Cadmus 1986). TX Psc is an irregular (type Lb) variable, and therefore the Mira-type pulsation mode cannot be at work in this star. Any shock waves that form in the Lb-variable, N-type carbon stars must do so at a low enough density (hence high enough in the atmosphere) to prevent Balmer lines from becoming observable. Indeed, Mira-type N stars do show Balmer lines, and Orlati (1987) has used these lines in the investigation of the "violet opacity problem" in these types of carbon stars. However, it is unlikely that shocks originate deep in the photosphere in the irregular and semiregular carbon stars. The formation of a shock will alter the temperature-density structure found in this paper, since hydrostatic equilibrium is assumed at all depths in this mode. A hydrodynamic calculation coupled with non–LTE radiative transfer calculations would be very beneficial and is currently under progress for Mira-type variables.

Obviously more data are needed for this star to test the uniqueness of this chromospheric model. A series of 15 hr ultraviolet spectra of the Mg II lines spread out over a few months could confront the question of the time variability of the chromosphere. TX Psc is a variable star, and the Mg II lines in low-resolution *IUE* spectra have been seen to vary in flux by a factor of 8 (Johnson *et al.* 1986). Unfortunately, the Mg II lines were just within reach of the high-resolution spectrograph on board *IUE* when these lines were at their peak flux level on the low-resolution *IUE* spectra. It is unlikely that *IUE* will be

able to gather further information on this star at high resolution.

Future work will investigate the effects of sphericity on the emergent flux (note that the Mg II emission is formed $0.07R_*$ above the continuum emitting regions) and will model the circumstellar shell surrounding TX Psc. The detailed study of chromospheric heating mechanisms cannot be started until non–LTE calculations of Fe and CO are completed, since both of these species are important cooling mechanisms (Johnson 1982; Carpenter 1987). Until high-resolution spectra of chromospheric indicators of the fainter cool carbon stars are available (i.e., by the Goddard high-resolution spectrograph aboard the Hubble Space Telescope), little progress can be made in semiempirical chromospheric modeling of other N-type stars. Since low-resolution *IUE* spectra of the sample of these stars are similar, this model for TX Psc should be fairly representative of chromospheres of these cool stars.

The *IUE* observations and reductions were supported by NASA grant NAG 5-182. The synthetic spectra calculations and computer graphics were supported by Indiana University through the Wrubel Computing Center. All of this support is appreciated. We are grateful to many friends for enlightening discussions and to J. A. Brown, J. A. Eaton, and P. G. Judge—as well as to an anonymous referee—for helpful comments on the manuscript.

## REFERENCES

Aaronson, M., and Mould, J. 1985, *Ap. J.*, **288**, 551.
Abt, H. A., and Biggs, E. S. 1972, *Bibliography of Stellar Radial Velocities* (New York: Latham).
Avrett, E. H., and Johnson, H. R. 1984, in *Proc. Third Cambridge Conf. on Cool Stars, Stellar Systems, and the Sun*, ed. S. L. Baliunas and L. Hartmann (New York: Springer-Verlag), p. 330.
Avrett, E. H., and Loeser, R. 1984, in *Methods in Radiative Transfer*, ed. W. Kalkofen (Cambridge: Cambridge University Press), p. 341.
Aymar, M. 1978, *J. Phys. B*, **11**, 1413.
Aymar, M., Luc-Koenig, E., and Combet Farnoux, F. 1976, *J. Phys. B*, **9**, 1279.
Ayres, T. R., and Testerman, L. 1978, *Solar Phys.*, **60**, 19.
Baschek, B., and Scholz, M. 1982, in *Landolt-Börnstein, New Ser., Group VI*, Vol. **2b**, *Stars and Star Clusters*, ed. K. Schaifers and H. H. Voigt (Berlin: Springer-Verlag), p. 91.
Basri, G. S. 1980, *Ap. J.*, **242**, 1133.
Bidelman, W. P., and Pyper, D. M. 1963, *Pub. A.S.P.*, **75**, 389.
Bohlin, R. C., Savage, B. D., and Drake, J. F. 1978, *Ap. J.*, **224**, 132.
Brugel, E. W., Willson, L. A., and Cadmus, R. 1986, in *New Insights in Astrophysics: 8 Years of UV Astronomy with IUE*, ed. E. J. Rolfe (ESA SP-263), p. 213.
Carpenter, K. G. 1987, in *IAU Colloquium 94, Physics of the Formation of* Fe II *Lines outside LTE*, ed. R. Viotti, A. Vittone, and M. Friedjung (Dordrecht: Reidel), p. 95.
Catchpole, R. M., and Feast, M. W. 1985, in *Cool Stars with Excess of Heavy Elements*, ed. M. Jaschek and P. C. Keenan (Dordrecht: Reidel), p. 113.
Cohen, J. G., Frogel, J. A., Persson, S. E., and Elias, J. H. 1981, *Ap. J.*, **249**, 481.
Eaton, J. A., and Johnson, H. R. 1988, *Ap. J.*, **325**, 355.
Eaton, J. A., Johnson, H. R., O'Brien, G. T., and Baumert, J. H. 1985, *Ap. J.*, **290**, 276.
Eriksson, K., Gustafsson, B., Johnson, H. R., Querci, F., Querci, M., Baumert, J. H., Carlsson, M., and Olofsson, H. 1986, *Astr. Ap.*, **161**, 305.
Faulkner, D. R., Honeycutt, R. K., and Johnson, H. R. 1988, *Ap. J.*, **324**, 490.
Frisch, H. 1980, *Astr. Ap.*, **83**, 166.
Grady, C. A. 1987, *IUE/NASA Newsletter*, No. 32, p. 99.
Hartmann, L., and Avrett, E. H. 1984, *Ap. J.*, **284**, 238.
Hubený, I. 1985, *Astr. Ap.*, **145**, 461.
Hudson, R. D., and Carter, V. L. 1967, *J. Opt. Soc. Am.*, **57**, 651.
Johnson, H. R. 1982, *Ap. J.*, **260**, 254.
———. 1987, in *Fifth Cambridge Workshop on Cool Stars, Stellar Systems, and the Sun*, ed. J. L. Linsky and R. E. Stencel (New York: Springer-Verlag), p. 399.
Johnson, H. R., Baumert, J. H., Querci, F., and Querci, M. 1986, *Ap. J.*, **311**, 960.
Johnson, H. R., and Luttermoser, D. G. 1987, *Ap. J.*, **314**, 329.
Johnson, H. R., Luttermoser, D. G., and Faulkner, D. R. 1988, *Ap. J.*, **332**, 421.
Johnson, H. R., and O'Brien, G. T. 1983, *Ap. J.*, **265**, 952.
Judge, P. D. 1989, in *IAU Colloquium 106, Evolution of Peculiar Red Giant Stars*, ed. H. R. Johnson and B. Zuckerman (Cambridge: Cambridge University Press), p. 303.
Kelm, S., and Schulter, D. 1962, *Zs. Ap.*, **56**, 78.
Lambert, D. L., Gustafsson, B., Eriksson, K., and Hinkle, K. H. 1986, *Ap. J. Suppl.*, **62**, 373.
Langhoff, P. W., Sims, J. S., and Corcoran, C. T. 1974, *Phys. Rev. A*, **10**, 829.
Lennon, D. J., Dufton, P. L., Hibbert, A., and Kingston, A. E. 1985, *Ap. J.*, **294**, 200.
Luttermoser, D. G., Johnson, H. R., Avrett, E. H., and Loeser, R. 1987, in *Fifth Cambridge Workshop on Cool Stars, Stellar Systems, and the Sun*, ed. J. L. Linsky and R. E. Stencel (New York: Springer-Verlag), p. 167.
Orlati, M. A. 1987, *Ap. J.*, **317**, 819.
Peach, G. 1970, *Mem. R.A.S.*, **73**, 1.
Querci, F., and Querci, M. 1983, in *Proc. Japan-France Seminar on Active Phenomena in the Outer Atmosphere of the Sun and Stars*, ed. J.-C. Pecker and Y. Uchida (Paris: Collège de France), p. 140.
Richer, H. B. 1975, *Ap. J.*, **197**, 611.
Ridgway, S. T., Wells, D. C., and Joyce, R. R. 1977, *A.J.*, **82**, 414.
Rothe, D. E. 1969, *J. Quant. Spectrosc. Rad. Transf.*, **9**, 49.
Scott, P., Kingston, A. E., and Hibbert, A. 1983, *J. Phys. B*, **16**, 3945.
Smith, V. V., and Lambert, D. L. 1985, *Ap. J.*, **294**, 326.
Stencel, R. E., Linsky, J. L., Brown, A., Jordan, C., Carpenter, K. G., Wing, R. F., and Czyzak, S. 1981, *M.N.R.A.S.*, **196**, 47P.
Tarafdar, S. P., and Vardya, M. S. 1973, *M.N.R.A.S.*, **163**, 261.
Tsuji, T. 1981, *J. Ap. Astr.*, **2**, 95.
Vernazza, J. E., Avrett, E. H., and Loeser, R. 1973, *Ap. J.*, **184**, 605.
———. 1976, *Ap. J. Suppl.*, **30**, 1.
———. 1981, *Ap. J. Suppl.*, **45**, 635.
Victor, G. A., and Dalgarno, A. 1969, *J. Chem. Phys.*, **50**, 2535.
Walker, A. R. 1980, *M.N.R.A.S.*, **190**, 453.
White, N. M., and Feierman, B. H. 1987, *A.J.*, **94**, 751.
Yamashita, Y. 1972, *Ann. Tokyo Astr. Obs.*, **13**, 169.
———. 1975, *Ann. Tokyo Astr. Obs.*, **15**, 47.

EUGENE H. AVRETT and RUDOLF LOESER: Center for Astrophysics, 60 Garden Street, Cambridge, MA 02138

HOLLIS R. JOHNSON: Astronomy Department, Indiana University, Bloomington, IN 47405

DONALD G. LUTTERMOSER: JILA, University of Colorado, Boulder, CO 80309